Electrochemical Mechanics of Metal Thin Films: Charge-Induced Reversible Surface Stress for Actuation

Chuan Cheng, Patrick S. Grant, and Lukas Lührs*

Dr. Chuan Cheng, Mr. Lukas Lührs
Institute of Materials Physics and Technology
Hamburg University of Technology
21073 Hamburg, Germany
E-mail: Chuan.Cheng@warwick.ac.uk

Dr. Chuan Cheng, Prof. Patrick S. Grant
Department of Materials
University of Oxford
Oxford, OX1 3PH, United Kingdom

Dr. Chuan Cheng,
WMG, University of Warwick
Coventry, CV4 7AL, United Kingdom

Keywords: electrochemical actuators, charge-induced surface stress, electrocapillary, metal thin films, nanoporous metals

The intrinsic charge-induced surface stress of Ni thin films during electrochemical reactions with an alkaline electrolyte is measured in situ. Surface stress induced by H absorption/desorption, α-$Ni(OH)_2$ formation, capacitive double-layer charging, the α- to β-$Ni(OH)_2$ transformation, and β-$Ni(OH)_2$/β-NiOOH redox reactions are identified, and each provided additive contributions to the overall stress state. Surface stresses are magnified in high surface area nanoporous Ni because local stress relaxation mechanisms are restricted when compared with a smooth Ni film. Ni film reversible tensile/compressive surface stresses correlates with anodic/cathodic potential scanning but with an opposite trend to that of a less reactive Au film. Surface stresses in the Ni films are up to 40 times that of Au films and suggest the possibility of using controlled surface stress generation for electrochemical actuation.

The measurement of electrode surface stresses induced by electrochemical processes at an electrode/electrolyte interface provides a method to probe the underlining atomistic processes and chemical changes related to charge transfer.[1] These surface stresses are also of critical importance in the thermodynamics of electrode surfaces, including aspects of surface reconstruction, self-organization, electrocatalysis, and electrochemical actuation.[2] Investigations of electrode surface stress have mainly concerned noble metals where the surface stress is induced by sub-monolayer adsorbates in an electrochemical double layer, which changes the electron distribution of surface atoms and induces reversible elastic strain, with reversible surface stresses of the order of 1 N m^{-1}, for Au, Pt, Pd, Ag, and Ir noble metals in various electrolytes.[3]

Investigation of surfaces stress in more chemically active transition metals, such as Ni, Co, Mn, are by comparison rare. The electrode/electrolyte interfaces of transition metals are intrinsically different from noble metals because more complex, higher strain and stress pseudocapacitive reactions may take place, rather than simply sub-monolayer adsorbates.[4] For example, the charge-induced reversible strain measured in nanoporous Ni has been shown to be one order of magnitude larger than that of a similar nanoporous noble metal[5] with resulting surface distortions observable with the naked eye.[6] As we show below, in situ measurement of surface stress, even in complex cases, can resolve sufficient detail that specific reactions can be deconvoluted and isolated. We also demonstrate that these surface stress effects can be enhanced by a nanoporous surface morphology, which may provide an opportunity for the development of electrochemical microactuators based on low cost transition metals.[3b, 7]

The charge-induced surface stress of a Ni film sputtered onto a Si wafer substrate was measured in situ by a multiple-beam optical stress sensor (MOSS) system combined with an electrochemical cell (**Figure 1**a).[8] During electrochemical reactions, if the interatomic distance of the film tends to contract but is restricted by the substrate, a tensile stress is developed in the film and the system is bowed into a concave shape on the Ni side (Figure 1b).

If the film tends to expand but is again restricted by the substrate, a compressive stress is developed in the film and the system bows on the convex side (Figure 1c).

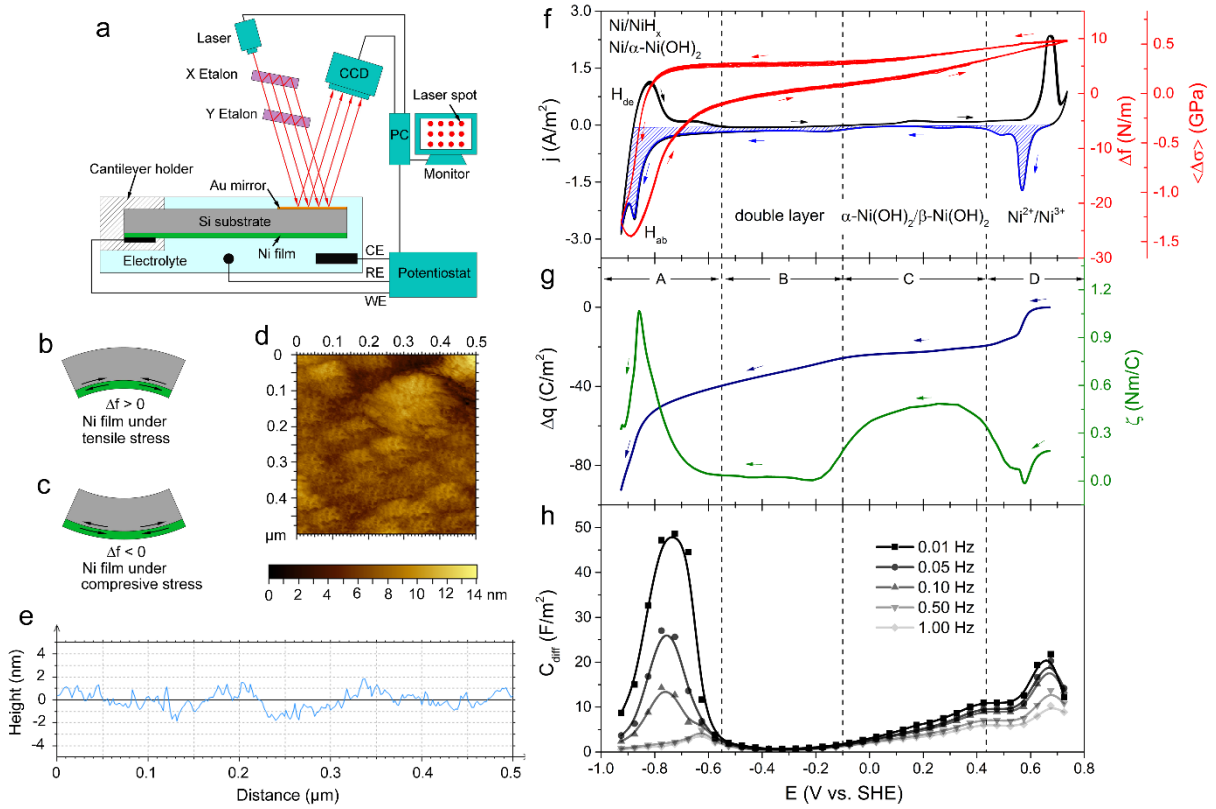

Figure 1. (a) Illustration of the experimental set-up for the in situ measurement of surface stress of a Ni thin film. Geometric changes of the cantilever when the Ni film is under (b) tensile and (c) compressive stresses. (d) Scanning tunneling microscope image of the sputtered Ni film and (e) the associated surface roughness profile. (f) Cyclic voltammetry of a Ni film at 5 mV s^{-1} in 1M NaOH (left axis), induced surface stress change Δf, and mean biaxial stress change $\langle\Delta\sigma\rangle$ (right axis). (g) Charge density integrated for a reduction process (blue region in (f)), and the corresponding surface stress-charge coefficient ς (right axis) against potential E. (h) Differential capacitance C_{diff} against potential at frequencies from 0.01 to 1.00 Hz.

From Stoney's equation,[9] the surface stress of the Ni film is given as:

$$\Delta f = \langle\Delta\sigma\rangle h_f = \frac{Y_s h_s^2 \cos\alpha}{12(1-\nu_s)Ln}\frac{\Delta d}{d_0} \qquad (1)$$

where $\langle\Delta\sigma\rangle$ is the change of mean biaxial stress of the film; h_f (= 18 nm) and h_s (= 200 μm) are the thickness of the film and the substrate, respectively; Δd is the change of the reflected beam spacing with respect to the initial beam spacing d_0; $\Delta d/d_0$ is the ratio measured by the MOSS system; Y_s (= 130.2 GPa) and ν_s (= 0.279) are Young's modulus and Poisson's ratio of the Si

substrate, respectively; n (= 1.33) is the refractive index of the electrolyte; α (= 3°) is the incident beam angle; and L (=105 cm) is the distance between the cantilever and the CCD camera. In Equation (1), Δf with units of N m^{-1}, is typically referred to as the "surface stress" in the literature but is more strictly the mean film stress × film thickness product.[10] Further details were provided in the supporting information (SI).

Scanning tunneling microscopy (STM) investigations of the as-sputtered Ni film showed a comparatively smooth surface with a mean height variation of ± 2 nm (Figures 1d-e) and electrode surface area of 3.2 cm^2 used in subsequent current areal density determination. The film thickness was approximately 18 nm measured by a spectroscopic ellipsometer (Figure S1).

Over six successive cyclic voltammetry (CV) cycles in Figure 1f, both current and induced Δf were highly reversible and four different electrochemical processes could be distinguished,[11] which provided additive contributions to the overall surface stress. During negative potential scanning starting from -0.550 to -0.925 V in region A of Figure 1f, H absorption[12] led to a sharp drop in surface stress from 5.4 N m^{-1} to -23.3 N m^{-1} and contributed ~80% of the overall surface stress of 35.9 N m^{-1}. The right hand side of Figure 1f also shows the mean biaxial stress of the film obtained from $\langle\Delta\sigma\rangle = \Delta f/h_f$ reached an overall amplitude of 2.0 GPa. The surface stress-charge coupling coefficient ($\varsigma = df/dq$, where q is the charge density), on the right hand side of Figure 1g, reached a maximum of ς = 1.07 Nm C^{-1} at -0.858 V during H adsorption, and similar to H absorption in other metals e.g. Pd (ς = 1.4 ± 0.2 Nm C^{-1}),[13] Pd (ς = 1.2 Nm C^{-1}),[14] and Pt (ς = 1.5 Nm C^{-1}).[15] Absorbed H typically occupies octahedral lattice sites to form β-NiH, which has a lattice constant 3.731 Å and 5.7% larger than that of Ni.[16] At a scan rate of 1 mV s^{-1}, the atomic ratio of H/Ni can reach ~0.5 and induce a compressive biaxial stress ~2.6 GPa in the Ni film (see SI).

As the scanning was switched to the positive direction from -0.925V, the surface stress in Figure 1f was partially relieved by H desorption at -0.550V because a Ni → α-Ni(OH)$_2$ reaction

took place at the same time,[11] as indicated by the corresponding current plateau from -0.716 to -0.614 V. α-$Ni(OH)_2$ formation induced surface expansion and partially compensated for the H desorption induced contraction. Differential capacitance ($C_{diff} = Y''/\omega$, where Y'' is the imaginary part of the admittance measured by electrochemical impedance spectroscopy and ω is angular frequency)[17] peaked at -0.725V corresponding to the α-$Ni(OH)_2$ formation and H desorption (Figure 1h). The strong frequency dependence of C_{diff} in Figure 1h suggested that C_{diff} was made up of both double layer capacitance and absorption capacitance.[17]

The flat current in region B was attributed to the capacitive double-layer behaviour, where surface stress increased linearly with potential (Figure 1f).[3b] C_{diff} was at a minimum of 40 µF cm^{-2}, which was consistent with the double layer capacitance of oxidized Ni (40-60 µF cm^{-2}).[18] In region C, an anodic current peak at 0.165V corresponded to the α-$Ni(OH)_2$ to β-$Ni(OH)_2$ transformation and was accompanied by lattice shrinkage and thus an increase in surface stress.[19] In region D, an oxidation peak at 0.672V and a reduction peak at 0.568V were attributed to the redox reaction β-$Ni(OH)_2 \leftrightarrow \beta$-NiOOH. The forward reaction leads to a lattice shrinkage,[20] again, with a corresponding increase in surface stress

For comparison, we synthesized 3D millimeter-sized nanoporous Ni samples by dealloying of Mn from a single phase $Ni_{30}Mn_{70}$ solid solution.[5a] **Figure 2**a and 2b show photos of the $Ni_{30}Mn_{70}$ precursor ingot and the corresponding dealloyed nanoporous Ni, respectively. The XRD pattern of the dealloyed sample confirmed fcc Ni (Figure 2c), while the TEM image in Figure 2d confirmed a nanoporous structure with Ni ligament sizes of 13 ± 3 nm between pores.

The electrochemically active surface area of the nanoporous Ni was determined using the behaviour of the much smoother Ni film as follows. First, the charge transferred during the reduction of β-NiOOH $\rightarrow \beta$-$Ni(OH)_2$ was obtained by integrating the CV of the Ni film in the region indicated by the slashed lines in Figure 2e. Then, by assuming that the same charge was

transferred per unit area for nanoporous Ni and film Ni at 1 mV s^{-1}, the electrochemically active surface area α_m of nanoporous Ni could be estimated as 9.2 m^2 g^{-1}.

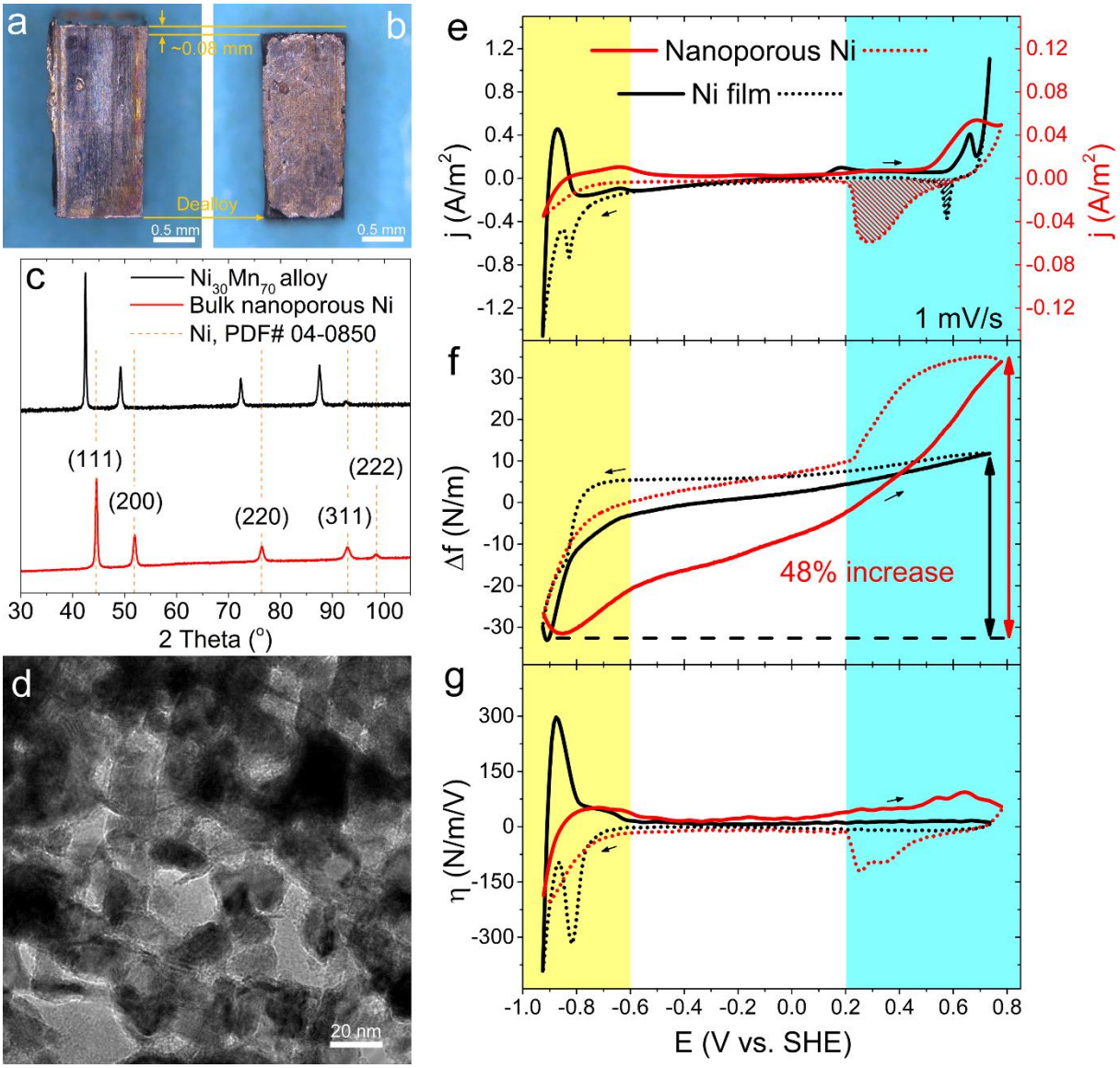

Figure 2. Photograph of (a) $Ni_{30}Mn_{70}$ alloy precursor ingot and (b) the corresponding dealloyed nanoporous Ni; (c) XRD pattern of $Ni_{30}Mn_{70}$ and nanoporous Ni compared with a reference Ni pattern (PDF# 04-0850). (d) TEM image of the dealloyed nanoporous Ni. (e) cyclic voltammetry of a Ni film (black) and nanoporous Ni (red) at 1 mV s^{-1} in 1 M NaOH electrolyte; (f) Charge-induced surface stress of the Ni film was measured by the MOSS system and Equation 1. The nanoporous Ni surface stress determined from the dilatometry strain measurement and Equation 3. (g) Derivative of surface stress with respect to potential, in which the derivative of the cathodic scan was multiplied by -1 (dotted curve) to clearly separate the forward and backward scan data.

Because the dealloyed Ni was bulk rather than a film, charge-induced dimensional change during CV at the same scan rate as applied to the films was measured instead by dilatometry.

The provided a macroscopic strain $\varepsilon = \Delta l/l_0$, where l_0 is the original length of the sample and Δl is the length change i.e. the MOSS system was used for thin film Ni and dilatometry was used for bulk nanoporous Ni.

Dilatometry strain $\varepsilon = \Delta l/l_0$ was then converted to an equivalent surface stress Δf using the capillary equation derived by Weissmüller and Cahn[21]:

$$3V_s\langle\Delta P\rangle_V = 2A\langle\Delta f\rangle_A \quad (2)$$

where A is the total wetted surface area, V_s is the total volume of solid, P is the volumetric mean of the pressure, f denotes surface stress, and the $\langle\rangle$ brackets denote their respective averages and assuming a linear elastic response, $\Delta P = -K\Delta V_s/V_s$, where K (= 180 GPa) is the bulk modulus of the solid Ni. The volume change of the solid ΔV was scaled with the macroscopic length change of nanoporous structure by $\Delta V_s/V_s = 3\Delta l/l_0$. Substituting these relations into Equation 2, we obtain the surface stress-strain relationship for the nanoporous Ni:[22]

$$\Delta f = -\frac{9K}{2\rho\alpha_m}\varepsilon \quad (3)$$

where α_m (= A/m) is the specific surface area of the nanoporous Ni, m is the solid mass, and ρ is the density of solid Ni.

The current peaks for nanoporous Ni were comparatively broad due to relatively sluggish ion transport within the tortuous nanoporous structure (Figure 2e) compared with the film Ni; accordingly, the surface stress in nanoporous Ni had a larger positive/negative scan hysteresis (Figure 2f). The magnitude of charge-induced surface stress in nanoporous Ni (66.6 N m^{-1}) was 48% larger than that of film Ni (44.9 N m^{-1}), indicating an amplification of surface stress.

In Figure 2e, the significant differences between the nanoporous Ni and film Ni the CV curves relate to the electrode morphology – nanoporous or smooth. The nanoporous electrode has a high tortuosity and surface area and its effect on the effective ion diffusion coefficient D_{eff} can be estimated[23] from $D_{eff} = D/\tau^2$, where D is the diffusion coefficient in the bulk electrolyte and τ is the electrode tortuosity. Evidently, the effective ion diffusion coefficient for the

nanoporous electrode must be lower than that of the smooth electrode. This reduced ion diffusion coefficient then decreased the peak current of CV curves and increased the peak width, as previously described by Equations (6.4.6) and (6.4.7) in Ref. [24]. In addition, the more sluggish ion diffusion within the nanoporous Ni may restrict the H lattice absorption compared with the Ni film at the same scan rate, which had more obvious H absorption /desorption peaks at the negative potential end.

During the β-$Ni(OH)_2 \rightarrow \beta$-NiOOH reaction (> 0.2V), surface stress in the nanoporous Ni increased sharply to 34.7 N m^{-1} and contributed 52% of the overall stress, which was more than three times that of film Ni (16%). The surface stress-voltage coupling coefficient was defined as $\eta = df/dE$ and is plotted in Figure 2g to show a pair of strong η peaks corresponding to the redox reactions for nanoporous Ni. η was larger for the nanoporous Ni because its highly curved, torturous geometry restricted local strain relaxation whereas strain was more readily relaxed in the smooth Ni film.

In addition, the scan rate of the CV will affect the strain and stress amplitude of Ni-based electrochemical actuators, which has been reported in our pervious publications, such as Figs. 2e and 3a in Ref. [5a] and Fig. 3b in Ref. [6a]. Similar tendencies have been reported by others, such as Fig. 2g in Ref. [5b]. These papers showed that the strain amplitude decreased quickly with increasing scan rates. However, the signs of the strain did not change, only the amplitude. The origin of this scan rate dependence is because the actuation of the Ni-based material arises from both pseudocapacitive charging and double-layer capacitive charging. The former process has faradic reactions that store more charge, and contribute most of the actuation strain/stress at low CV scan rates. However, the pseudocapacitive process becomes restricted by mass-transport with increasing scan rate and its relative contribution to actuation quickly diminishes. In the contrast, the charge accumulated in the double-layer is a capacitive process with a time constant below a millisecond,[25] and is consequently much less affected by the CV scan rates.

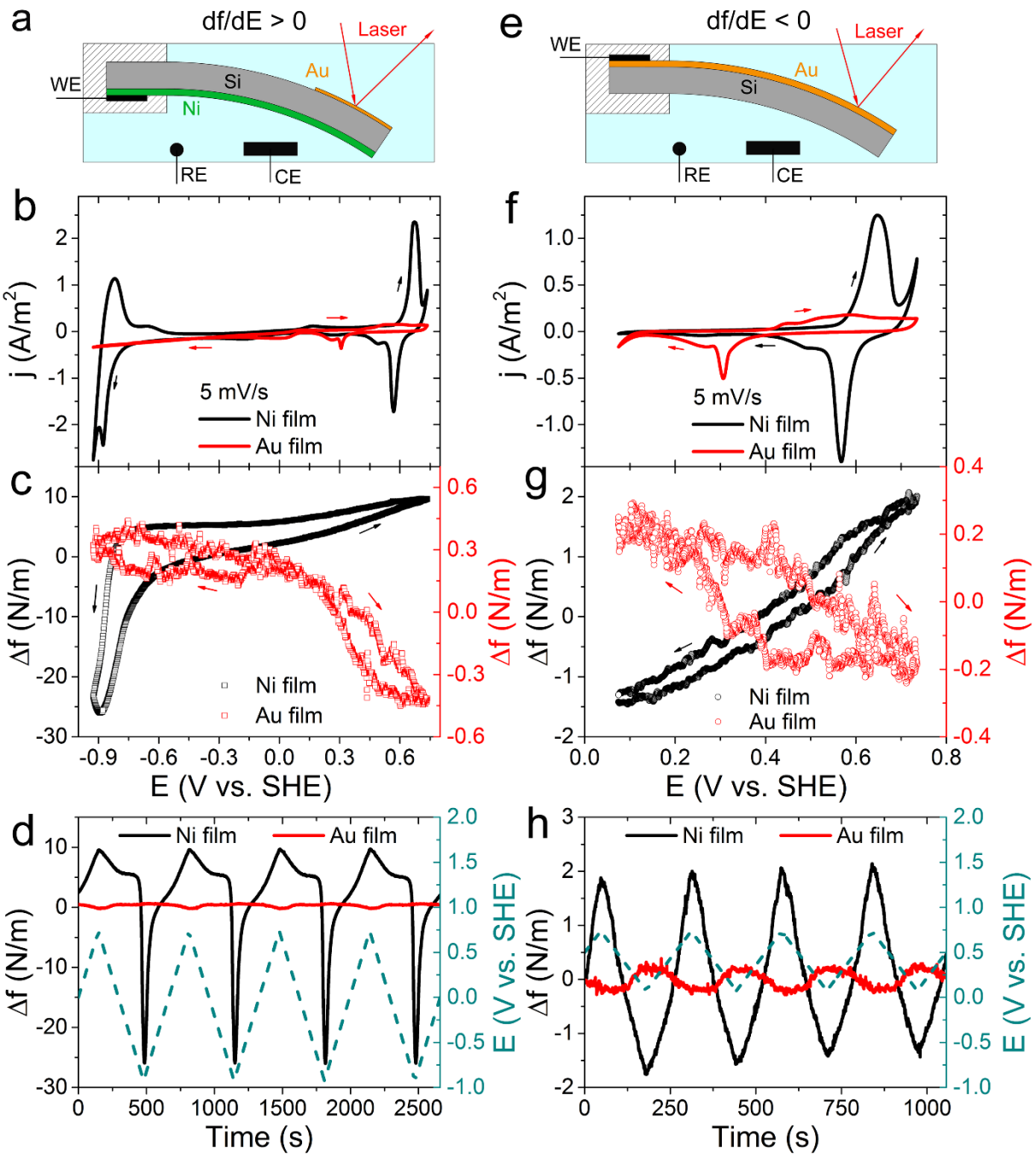

Figure 3. Comparison of the charge-induced surface stresses in Ni and Au thin films during cyclic voltammetry. (a, e) Illustration of the cantilever bending during positive potential scanning with Ni and Au thin films as working electrodes, respectively. Cyclic voltammetry of Ni and Au thin films at 5 mV s^{-1} in 1M NaOH electrolyte within (b) [-0.925, 0.735] V vs. SHE; and (f) [0.075, 0.735] V vs. SHE. (c, g) Surface stress against potential corresponding to (b, f), respectively. (d, h) Surface stress (left) and potential (right) against time for cyclic scanning of the Ni and Au thin films.

As Au has been used widely as a model material for charge induced stress/strain investigations,[26] the intrinsic charge-stress coupling of Ni film was compared with a similar Au film (**Figure 3**). The current densities produced by the Au film were much smaller than Ni

in both the electrochemical stability potential region (Figure 3b) and the redox region (Figure 3f), which reflected the lower capacitance of Au. As a result, surface stress for Ni was approximately 40 times and 7 times that of Au in the corresponding surface stress plots in Figures 3c and 3g, respectively. These differences were reproducible during repeated cycles, as shown in Figures 3d and 3h.

There were no H absorption/desorption current peaks for Au contributing to strain (Figure 3b, red). In contrast, H absorption/desorption for Ni contributed approximately 80% of the resulting surface stress (Figure 3c, black). Even when surface processes only were considered, Au had a much smaller surface stress response than Ni (Figure 3g). The CV response of the Au film in Figure 3f can be separated into three regions:[27] (i) a capacitive double layer region (< 0.1 V); (ii) a non-oxide region (0.1 to 0.45V), and (iii) an oxide-region (> 0.45V). The non-oxide region was attributed to the reversible formation of electrosorbed OH- species,[28] with a charge transfer of 2.39 C m^{-2} obtained from CV, which corresponded to a monolayer of adsorbed OH- species on (111) plane (theoretically, 2.23 C m^{-2}), consistent with reports that sputtered Au films on (001)-oriented Si wafers typically have a (111)-oriented surface.[8] With potential increasing to the oxide-region, a broad anodic peak was associated with oxidation of $Au(OH)_{ad}$ towards $Au(OH)_3$,[29] with a total charge transfer of 7.58 C m^{-2} that corresponded to the production of $Au(OH)_{3.4}$. However, considering possible roughness of the Au film, which was neglected in the charge density evaluation, the reaction product may be close to a monolayer of $Au(OH)_3$ formation (> 0.45V).

In the case of the Ni film, for hexagonal structured β-$Ni(OH)_2$ sheets with a Ni-Ni interatomic distance of 3.13 Å,[18] the transferred charge for a monolayer of redox reaction was estimated at 1.89 C m^{-2}. However, there was a transfer charge of 16.88 C m^{-2} in the redox region here, approximating to 9 layers of β-$Ni(OH)_2$. By assuming (001) oriented β-$Ni(OH)_2$ at the Ni surface, the thickness of the oxide passive layer was approximately 4.1 nm, which agrees reasonably well with prior XPS measurements.[30] Therefore, a monolayer of Au was oxidized

while 9 layers of β-Ni(OH)$_2$ were oxidized in the same potential region of Figure 3f, which led to the 7 times measured difference in charge-induced surface stress in Figure 3g.

In terms of the surface stress-voltage coupling coefficient $\eta = df/dE$, Figures 3d and 3h show that Δf for Ni was in-phase with potential ($df/dE > 0$) while Δf for Au was out-of-phase with potential ($df/dE < 0$). From Figure 3g, a linear best-fit of the surface stress to potential gave η = 5.36 N m^{-1} V^{-1} for the Ni film and η = -0.66 N m^{-1} V^{-1} for the Au film. Thus, during positive scanning, the Ni film contracted whereas Au film expanded, as illustrated in Figures 3a and 3e. The difference in signs of η originated from the nature of the metal surface i.e. whether it was covered with oxide ("+" sign) or a "clean" metal surface ("-" sign). At the onset of the oxidation reaction for the redox pair β-Ni(OH)$_2$/β-NiOOH, β-Ni(OH)$_2$ was already present on the Ni surface while Au was not yet oxidized. Here, 'clean' metal surface means a surface without (anodic) oxide coverage. Before charging of a clean Au surface, the bonding strength between surface atoms is stronger compared with the bulk due to the redistribution of surface electrons towards in-plane and inner bonds, as a result, the equilibrium interatomic distance of surface atoms is reduced compared with the bulk atoms (surface contraction).[31] Upon positive charging, the excess positive charge reduces surface electron density, and the interatomic distance is increased, which results in localized surface expansion. This actuation mechanism is different from the case of Ni with a surface oxide. The surface stress of Ni is mainly attributed to pseudocapacitive processes with reactants consumption and products formation on the surface (leading to lattice mismatch or lattice volume change) rather than capacitive charge accumulation or release, as explained for Figure 1f.

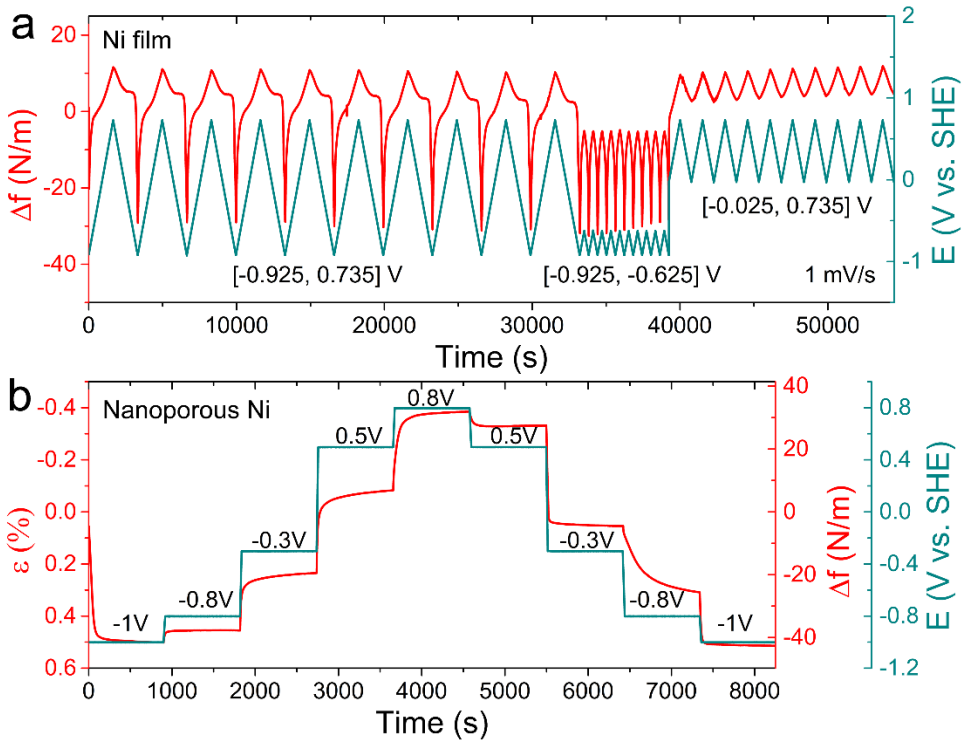

Figure 4. (a) The variation of surface stress with time for a Ni film under cyclic potential scanning for different potential windows at 1 mV s^{-1} in 1M NaOH electrolyte. (b) The variation of strain in nanoporous Ni (left) as a function of time and the corresponding surface stress (right) at different potential steps. Please note that the red curve plots both strain and stress, which are linearly related by Equation (3), with the resulting different scales and units given on the left and right hand side vertical axes respectively.

Figure 4a shows the highly reversible electrochemical actuation of a Ni film during cyclic potential scanning at 1 mV s^{-1} over 15 hours. Surface stress contributions from different potential regions could again be easily separated and reproduced in successive cycles. Figure 4b demonstrates that as the potential applied to the Ni film jumped step-wise, the induced strain in nanoporous Ni stabilized after approximately 2 min. This actuation stability is critical for actuator applications that require fixed strain without drift overtime and typically suffered by polymer-based low-voltage actuators such as ionic electroactive polymers,[32] or by nanoporous noble metal-based actuators due to ligament coarsening.[26a]

In summary, the charge-induced surface stress of Ni thin films due to electrochemical processes in an alkaline electrolyte was measured in situ by a MOSS system combined with an electrochemical cell. A non-linear, positive-signed surface stress-charge coefficient over a wide potential window comprised the additive effect of different surface stress generation

mechanisms. Compared with the Ni film, bulk nanoporous Ni had higher surface stresses due to the highly curved tortuous geometry of the electrolyte/Ni interface that restricted local stress relaxation. Compared with Au thin films measured under the same conditions, the induced surface stresses in Ni film were ~40 times of Au film within the accessible potential region, and ~7 times of Au film within the redox region. These significant differences highlighted the advantage of Ni over noble metals for large surface stress generation for possible electrochemical actuation applications.

Supporting Information
Supporting Information is available from the Wiley Online Library or from the author.

Acknowledgements
C.C. thanks the Alexander von Humboldt Foundation, Germany, for a research fellowship. This work received the financial support of the DFG via SFB "M3" subproject B2 and UK Engineering and Physical Science Research Council grant EP/P005411/1 (SELFIES). We thank Jörg Weissmüller for discussion and comments, Jürgen Markmann for assistance with spectroscopic ellipsometer, Shan Shi for assistance with magnetron sputtering, and Anastasia Straßer for assistance with STM.

Received: ((will be filled in by the editorial staff))
Revised: ((will be filled in by the editorial staff))
Published online: ((will be filled in by the editorial staff))

References

[1] a) W. Haiss, *Rep. Prog. Phys.* **2001**, *64*, 591; b) R. C. Cammarata, *Prog. Surf. Sci.* **1994**, *46*, 1; c) R. C. Cammarata, K. Sieradzki, *Annu. Rev. Mater. Sci.* **1994**, *24*, 215.

[2] a) H. Ibach, *Surf. Sci. Rep.* **1997**, *29*, 195; b) P. Müller, A. Saúl, *Surf. Sci. Rep.* **2004**, *54*, 157; c) J. Weissmüller, K. Sieradzki, *MRS Bull.* **2018**, *43*, 14.

[3] a) P. J. Feibelman, *Phys. Rev. B* **1997**, *56*, 2175; b) J. Weissmüller, R. N. Viswanath, D. Kramer, P. Zimmer, R. Würschum, H. Gleiter, *Science* **2003**, *300*, 312; c) V. Fiorentini, M. Methfessel, M. Scheffler, *Phys. Rev. Lett.* **1993**, *71*, 1051; d) Q. B. Deng, J. Weissmuller, *Langmuir* **2014**, *30*, 10522.

[4] C. Cheng, A. H. W. Ngan, *ACS Nano* **2015**, *9*, 3984.

[5] a) C. Cheng, L. Lührs, T. Krekeler, R. Ritter, J. Weissmüller, *Nano Lett.* **2017**, *17*, 4774; b) Q. Bai, Y. Wang, J. Zhang, Y. Ding, Z. Peng, Z. Zhang, *J. Mater. Chem. C* **2016**, *4*, 45.

[6] a) C. Cheng, J. Weissmüller, A. H. W. Ngan, *Adv. Mater.* **2016**, *28*, 5315; b) D. Kramer, R. N. Viswanath, J. Weissmüller, *Nano Lett.* **2004**, *4*, 793.

[7] K. W. Kwan, S. J. Li, N. Y. Hau, W.-D. Li, S. P. Feng, A. H. W. Ngan, *Sci. Robot.* **2018**, *3*, eaat4051.

[8] M. Smetanin, R. N. Viswanath, D. Kramer, D. Beckmann, T. Koch, L. A. Kibler, D. M. Kolb, J. Weissmüller, *Langmuir* **2008**, *24*, 8561.

[9] a) G. G. Stoney, *Proc. R. Soc. A* **1909**, *82*, 172; b) Q. V. Overmeere, J. F. Vanhumbeeck, J. Proost, *Rev. Sci. Instruments* **2010**, *81*, 045106.

[10] J. A. Floro, E. Chason, S. R. Lee, R. D. Twesten, R. Q. Hwang, L. B. Freund, *J. Electron. Mater.* **1997**, *26*, 969.

[11] D. S. Hall, D. J. Lockwood, C. Bock, B. R. MacDougall, *Proc. R. Soc. A* **2015**, *471*, 20140792.

[12] S. A. S. Machado, L. A. Avaca, *Electrochim. Acta* **1994**, *39*, 1385.

[13] L. A. Kibler, A. M. El-Aziz, R. Hoyer, D. M. Kolb, *Angew. Chem. Int. Ed.* **2005**, *44*, 2080.

[14] R. N. Viswanath, J. Weissmüller, *Acta Mater.* **2013**, *61*, 6301.

[15] J. Weissmüller, R. N. Viswanath, L. A. Kibler, D. M. Kolb, *Phys. Chem. Chem. Phys.* **2011**, *13*, 2114.

[16] a) B. Predel, in *Chapter: H-Ni (Hydrogen-Nickel), in Ga-Gd – Hf-Zr* (Ed.: O. Madelung), Springer Berlin Heidelberg, Berlin, Heidelberg, **1996**, pp. 1-6; b) N. Takano, S. Kaida, *ISIJ International* **2012**, *52*, 263.

[17] V. D. Jovic, B. M. Jovic, *J. Electroanal. Chem.* **2003**, *541*, 1.

[18] D. S. Hall, Ph.D. thesis, University of Ottawa **2014**.

[19] R. S. McEwen, *J. Phys. Chem.* **1971**, *75*, 1782.

[20] M. B. J. G. Freitas, *J. Power Sources* **2001**, *93*, 163.

[21] J. Weissmüller, J. W. Cahn, *Acta Mater.* **1997**, *45*, 1899.

[22] J. Weissmüller, H. L. Duan, D. Farkas, *Acta Mater.* **2010**, *58*, 1.

[23] a) J. van Brakel, P. M. Heertjes, *Int. J. Heat Mass Tran.* **1974**, *17*, 1093; b) L. Shen, Z. Chen, *Chem. Eng. Sci.* **2007**, *62*, 3748.

[24] A. J. Bard, L. R. Faulkner, *Electrochemical Methods: Fundamentals and Applications*, John Wiley & Sons, New York, **2001**.

[25] J. Lück, A. Latz, *Phys. Chem. Chem. Phys.* **2018**, *20*, 27804.

[26] a) H. J. Jin, J. Weissmüller, *Science* **2011**, *332*, 1179; b) C. Stenner, L. H. Shao, N. Mameka, J. Weissmuller, *Adv. Funct. Mater.* **2016**, *26*, 5174; c) L. Lührs, B. Zandersons, N. Huber, J. Weissmüller, *Nano Lett.* **2017**, *17*.

[27] H. Angerstein-Kozlowska, B. E. Conway, B. Barnett, J. Mozota, *J. Electroanal. Chem.* **1979**, *100*, 417.

[28] R. Cordova O, M. E. Martins, A. J. Arvia, *Electrochim. Acta* **1980**, *25*, 453.

[29] R. Cordova O, M. E. Martins, A. J. Arvia, *J. Electrochem. Soc.* **1979**, *126*, 1172.

[30] H. W. Hoppe, H. H. Strehblow, *Surf. Interface Anal.* **1989**, *14*, 121.

[31] a) F. Weigend, F. Evers, J. Weissmüller, *Small* **2006**, *2*, 1497; b) H. J. Jin, S. Parida, D. Kramer, J. Weissmüller, *Surf. Sci.* **2008**, *602*, 3588.

[32] Y. Bar-Cohen, *Electroactive Polymer (EAP) Actuators as Artificial Muscles - Reality, Potential and Challenges*, 2nd ed., SPIE Press, **2004**.

The table of contents entry:
Charge-induced surface stress in Ni thin film and bulk nanoporous Ni leads to tensile stress in Ni film and volume shrinkage in bulk nanoporous Ni during charging, which is reversible during discharging. The nanoporous morphology restricts local stress relaxation and amplifies the charge-induced surface stress effect.

Keywords: electrochemical actuators, charge-induced surface stress, electrocapillary, metal thin films, nanoporous metals

Authors: C. Cheng,* P. S. Grant, and L. Lührs

Title: **Electrochemical Mechanics of Metal Thin Films: Charge-Induced Reversible Surface Stress for Actuation**

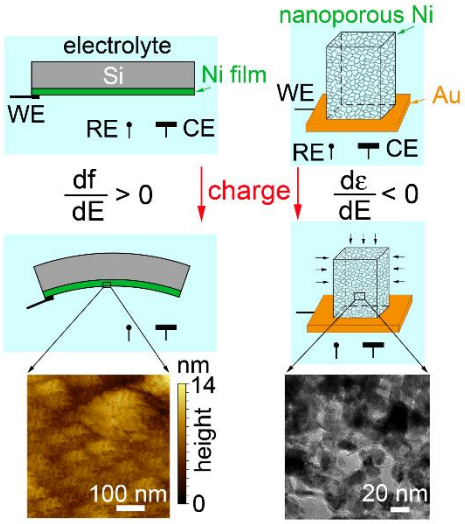

ToC Figure

Supporting Information

Electrochemical Mechanics of Metal Thin Films: Charge-Induced Reversible Surface Stress for Actuation

Chuan Cheng, Patrick S. Grant, and Lukas Lührs*

Dr. Chuan Cheng, Mr. Lukas Lührs
Institute of Materials Physics and Technology
Hamburg University of Technology
21073 Hamburg, Germany
E-mail: Chuan.Cheng@warwick.ac.uk

Dr. Chuan Cheng, Prof. Patrick S. Grant
Department of Materials
University of Oxford
Oxford, OX1 3PH, United Kingdom

Dr. Chuan Cheng,
WMG, University of Warwick
Coventry, CV4 7AL, United Kingdom

Experimental Procedures

Sample preparation. A 200 μm thick n-doped Si wafer with 100 nm thermal oxide coverage (CrysTech GmbH, Germany) was cut into 40 mm × 8 mm rectangles. A thin Ti film was first sputtered on one side of the Si wafer by magnetron sputtering (BESTEC GmbH, Germany) at 100 W for 5 min under 7 SCCM (standard cubic centimeter per minute) Ar flow rate with film growth rate 2 nm min^{-1} for the purpose of strong mechanical contact between Ni film and the substrate.[1] A Ni film was then sputtered at 100 W for 10 min under 7 SCCM Ar flow rate. The film growth rate of Ni was ~ 1.83 nm min^{-1} according to the film thickness against sputtering time relationship (Figure S1) where the film thickness was measured as a function sputtering time by a spectroscopic ellipsometer (M-2000F Spectroscopic Ellipsometer, J.A.Woollam Co. Inc.). Ni thin films were typically 18 nm in thickness. On the other side of the Si wafer, a Au thin film was sputtered at one end (area ~8 mm × 15 mm) to act as a mirror

for laser reflection. After sputtering, the edges of the sample (200 µm side) were slightly polished by sand paper to guarantee electric isolation which was checked by a multimeter between the Ni film on one side of the wafer and the Au mirror on the other side. Thus, when the Ni film was charged in the electrochemical cell, the Au mirror was not charged and did not contribute to any electrochemical process.

For electrochemical tests of Au films, Au was coated on one side of the Si wafer by magnetron sputtering at 50 W for 8 min under 7 SCCM Ar flow rate (film growth rate 10 nm min^{-1}).[1] This Au film acted as both working electrode and laser reflection mirror, while in this case the other side of the Si wafer had no other coating.

For electrochemical tests of bulk nanoporous Ni, a $Ni_{30}Mn_{70}$ alloy ingot was cast in an induction cold crucible furnace (Arcast) in Ar atmosphere from elemental Ni and Mn feedstock (> 99.99% pure, ChemPUR). The ingot was then annealed at 900 °C for 24 hours under vacuum and then quenched in water to obtained a single phase solid solution according to the phase diagram,[2] and confirmed by XRD (Figure 2c of the main text, black curve). The ingot was cut into 3D millimeter sized cuboids by a diamond wire saw. Nanoporous Ni was then synthesized by free corrosion of the cuboids in 0.2M $(NH_4)_2SO_4$ at 55°C for 20 to 30 hrs.

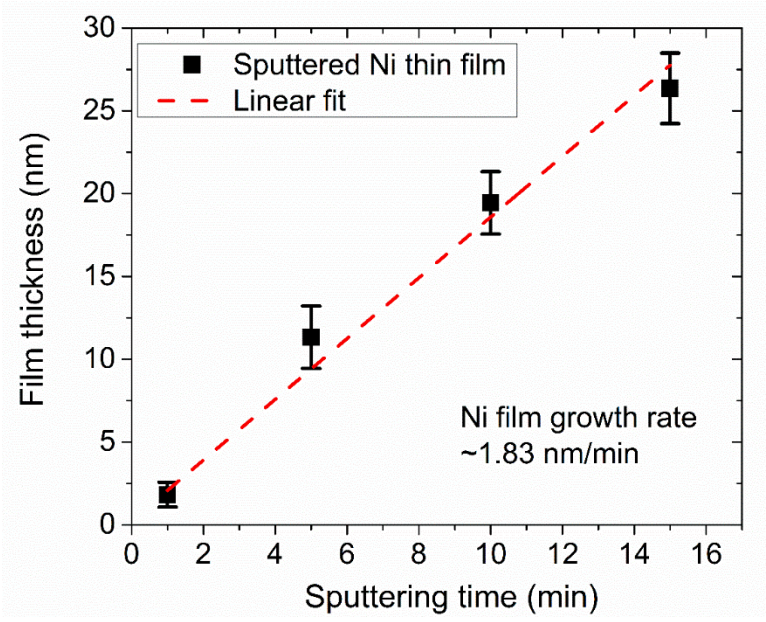

Figure S1. Relationship between Ni film thickness and magnetron sputtering time at 100 W with 7 SCCM Ar flow rate.

Setup for in-situ surface stress measurement of metal films. The charge-induced surface stress on the Ni or Au films was measured *in situ* by a multiple-beam optical stress sensor (MOSS) system (k-Space Associates Inc., USA)[3] during electrochemical processes. As illustrated in Figure 1a, the MOSS system utilized a solid state laser in conjunction with two orthogonal etalons to produce 3 × 4 arrays of parallel beams. The beams propagated through the electrolyte and were projected on to the Au mirror on the cantilever. The reflected beams were monitored by a charge coupled device (CCD) camera, and images transferred to a computer for measurements of the beam spacing with time. The beam spacing changed due to bending of the cantilever, induced by any changes of the surface stress.

For electrochemistry and stress measurement of Ni film (Figure 1a), the metal coated Si wafer with the Au mirror facing upwards was fixed at one end in a homemade electrochemical cell filled with 1M NaOH electrolyte. The Ni film was connected as the working electrode (WE) of the potentiostat (Autolab, PGSTAT302N) through a Au wire (0.25 mm in diameter). A Pt wire acted as a counter electrode (CE), and a home-made Ag/AgCl reference electrode (0.375 V vs. SHE in 1 M NaOH at room temperature, Figure S2) was inserted into the electrochemical cell just below the Ni film.

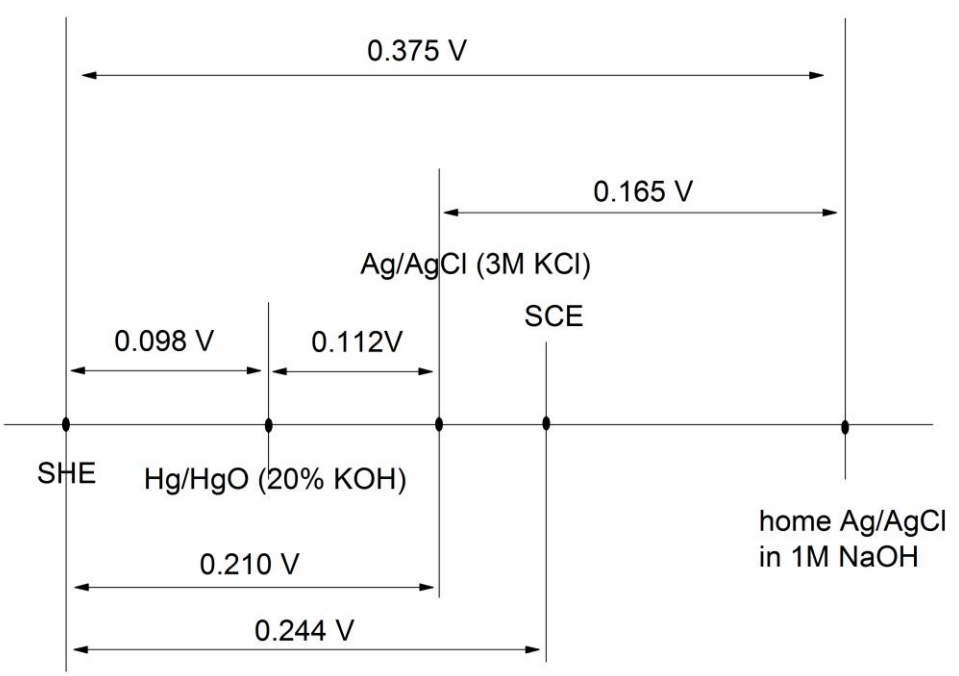

Figure S2. Illustration of home-made Ag/AgCl reference electrode against various common reference electrodes in 1M NaOH electrolyte. The home-made Ag/AgCl electrode was made by anodization of Ag wire (0.5 mm diameter, 99.99% pure) in 1M HCl solution at 0.9V for 120 seconds with another Ag wire as both counter and reference electrodes. The electrode potential was calibrated against a commercial Ag/AgCl (3M KCl) electrode (Sigma-Aldrich) in 1M NaOH solution (the same solution for electrolyte in this work). The potential of home-made electrode was stable at ~0.165 V vs. Ag/AgCl (3M KCl) even after 3 days of working.

Bending curvature determination. During cyclic voltammetry, electrochemical reactions took place on Ni film leading to a change in the Ni film surface stress change, and due to the constraint of the substrate, the cantilever then deflected. The change of bending curvature $\Delta\kappa$ of the cantilever can be expressed as:[4]

$$\Delta\kappa = \frac{\cos\alpha}{2Ln}\frac{\Delta d}{d_0} \qquad \text{(S1)}$$

where d_0 is the initial beam spacing; Δd is the change of beam spacing; n is the refractive index of the electrolyte; α is the incident beam angle; L is the distance between the cantilever and the camera. $\Delta d/d_0$ ratio was measured directly from the MOSS system. From Stoney's equation,[5] the change of mean biaxial stress of a thin film coated on a much thicker substrate can be expressed as

$$\langle \Delta\sigma \rangle = \frac{Y_s h_s^2}{6(1-v_s)h_f} \Delta\kappa \quad \text{(S2)}$$

where Y_s and v_s are Young's modulus and Poisson's ratio of the substrate, respectively; h_s and h_f are the thickness of the substrate and the film, respectively. Here, we use surface stress Δf to represent the stress state of the film.

$$\Delta f = \langle \Delta\sigma \rangle h_f \quad \text{(S3)}$$

As presented in the main text, for Ni films, the charge-induced stress can originate at three different depth positions: (i) at the film surface by adsorbed ions in an electrochemical double-layer; (ii) in the surface region (e.g. several nm) due to redox relations involving several mono-layers of nickel hydroxide formation; and (iii) in the film "bulk" by mobile H absorption/desorption, depending on the film thickness, the hydrogen diffusion coefficient, etc, and noting that nickel hydride formation may block further H uptake.[6] Although the detailed film stress distribution may be depth dependent, because the film thickness (18 nm) is much thinner than the substrate (200 μm) the Δf determined by experiment using Equation 1 can be considered the change of average surface stress.

Setup for in-situ strain measurement of** bulk **nanoporous metal. The linear charge-induced strain of bulk nanoporous Ni was measured *in situ* in an electrochemical cell, combined with a computer-controlled dilatometer (Linseis, L75 vertical dilatometer) and a potentiostat (Autolab, PGSTAT302N). A glass push rod was connected to the displacement sensor of the dilatometer with a small constant compressive pressure (~0.2 MPa) on the top surface of the sample in order to maintain a close contact. The electrochemical cell was filled with 1M NaOH electrolyte with the nanoporous Ni as the working electrode, a piece of carbon cloth as the counter electrode, and a commercial Hg/HgO reference electrode (0.098 V vs. SHE, Sensortechnik Meinsberg, Germany). All electrode potentials presented were converted to SHE.

Method to calculate differential capacitance. C_{diff} is calculated by the following equation according to Ref. [7] .

$$C_{diff} = \frac{Y''}{2\pi f} = \frac{Z''}{2\pi f[(Z'-R_s)^2+Z''^2]} \quad \text{(S4)}$$

where Y'' is the imaginary part of the electrode admittance, Y (= $1/Z$), where $Z = Z' + jZ''$, is the impedance. R_s is ohmic resistance determined from the high frequency intercept on Z' axis in the Z' vs. $-Z''$ diagram. Z was measured by electrochemical impedance spectroscopy with a potentiostat (Autolab, PGSTAT302N).

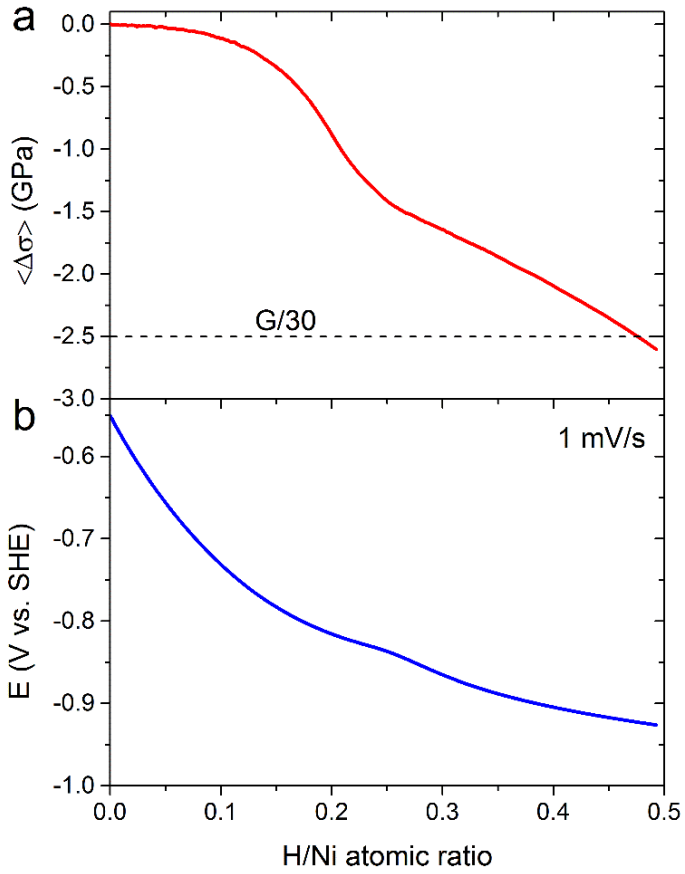

Figure S3. (a) H absorption induced change of mean biaxial stress <Δσ> in a Ni thin film as a function of H/Ni atomic ratio, where the H content was calculated from the measured charge during reduction process in cyclic voltammetry by Faraday's law. The H absorption was assumed to start at -0.55V vs. SHE (the left dash line in Figures 1f-h) until the end of the reduction processes (-0.925V vs. SHE). The horizontal dash line in (a) indicates the approximate theoretical shear strength of the Ni given by G/30 where G = 76 GPa is the shear modulus of Ni. (b) Electrode potential as a function of H/Ni atomic ratio.

Figure S3a shows the H absorption induced mean biaxial stress increased non-linearly with H uptake into the Ni film. In most of the potential region, under the lowest scan rate of 1mV s^{-1}, the induced biaxial stress was below the theoretical shear strength of the Ni. As the H/Ni ratio increased, β-nickel hydride could form, with fcc structure and a lattice constant of 3.731 Å, representing a 5.7% linear lattice expansion compared with Ni (3.530 Å).[8] The expansion of the film is restricted by the substrate and induced a compressive stress in the film. The stress was similar to that reported for H absorption into Nb films on a Si substrate.[9]

References

[1] V. Gopal, Master thesis, Technische Universität Hamburg, **2014**.

[2] N. A. Gokcen, *J. Phase Equilibria* **1991**, *12*, 313.

[3] a) M. Smetanin, Ph.D. Thesis, Universität des Saarlandes, **2010**; b) M. Smetanin, R. N. Viswanath, D. Kramer, D. Beckmann, T. Koch, L. A. Kibler, D. M. Kolb, J. Weissmüller, *Langmuir* **2008**, *24*, 8561.

[4] Q. V. Overmeere, J. F. Vanhumbeeck, J. Proost, *Rev. Sci. Instruments* **2010**, *81*, 045106.

[5] G. G. Stoney, *Proc. R. Soc. A* **1909**, *82*, 172.

[6] A. Pundt, R. Kirchheim, *Annu. Rev. Mater. Res.* **2006**, *36*, 555.

[7] V. D. Jovic, B. M. Jovic, *J. Electroanal. Chem.* **2003**, *541*, 1.

[8] N. Takano, S. Kaida, *ISIJ International* **2012**, *52*, 263.

[9] U. Laudahn, A. Pundt, M. Bicker, U. V. Hulsen, U. Geyer, T. Wagner, R. Kirchheim, *J. Alloys Comp.* **1999**, *293*, 494.

Supporting Information

Electrochemical Mechanics of Metal Thin Films: Charge-Induced Reversible Surface Stress for Actuation

Chuan Cheng, Patrick S. Grant, and Lukas Lührs*

Dr. Chuan Cheng, Mr. Lukas Lührs
Institute of Materials Physics and Technology
Hamburg University of Technology
21073 Hamburg, Germany
E-mail: Chuan.Cheng@warwick.ac.uk

Dr. Chuan Cheng, Prof. Patrick S. Grant
Department of Materials
University of Oxford
Oxford, OX1 3PH, United Kingdom

Dr. Chuan Cheng,
WMG, University of Warwick
Coventry, CV4 7AL, United Kingdom

Experimental Procedures

Sample preparation. A 200 μm thick n-doped Si wafer with 100 nm thermal oxide coverage (CrysTech GmbH, Germany) was cut into 40 mm × 8 mm rectangles. A thin Ti film was first sputtered on one side of the Si wafer by magnetron sputtering (BESTEC GmbH, Germany) at 100 W for 5 min under 7 SCCM (standard cubic centimeter per minute) Ar flow rate with film growth rate 2 nm min^{-1} for the purpose of strong mechanical contact between Ni film and the substrate.[1] A Ni film was then sputtered at 100 W for 10 min under 7 SCCM Ar flow rate. The film growth rate of Ni was ~ 1.83 nm min^{-1} according to the film thickness against sputtering time relationship (Figure S1) where the film thickness was measured as a function sputtering time by a spectroscopic ellipsometer (M-2000F Spectroscopic Ellipsometer, J.A.Woollam Co. Inc.). Ni thin films were typically 18 nm in thickness. On the other side of the Si wafer, a Au thin film was sputtered at one end (area ~8 mm × 15 mm) to act as a mirror for laser reflection.

After sputtering, the edges of the sample (200 µm side) were slightly polished by sand paper to guarantee electric isolation which was checked by a multimeter between the Ni film on one side of the wafer and the Au mirror on the other side. Thus, when the Ni film was charged in the electrochemical cell, the Au mirror was not charged and did not contribute to any electrochemical process.

For electrochemical tests of Au films, Au was coated on one side of the Si wafer by magnetron sputtering at 50 W for 8 min under 7 SCCM Ar flow rate (film growth rate 10 nm min^{-1}).[1] This Au film acted as both working electrode and laser reflection mirror, while in this case the other side of the Si wafer had no other coating.

For electrochemical tests of bulk nanoporous Ni, a $Ni_{30}Mn_{70}$ alloy ingot was cast in an induction cold crucible furnace (Arcast) in Ar atmosphere from elemental Ni and Mn feedstock (> 99.99% pure, ChemPUR). The ingot was then annealed at 900 ^{o}C for 24 hours under vacuum and then quenched in water to obtained a single phase solid solution according to the phase diagram,[2] and confirmed by XRD (Figure 2c of the main text, black curve). The ingot was cut into 3D millimeter sized cuboids by a diamond wire saw. Nanoporous Ni was then synthesized by free corrosion of the cuboids in 0.2M $(NH_4)_2SO_4$ at 55^{o}C for 20 to 30 hrs.

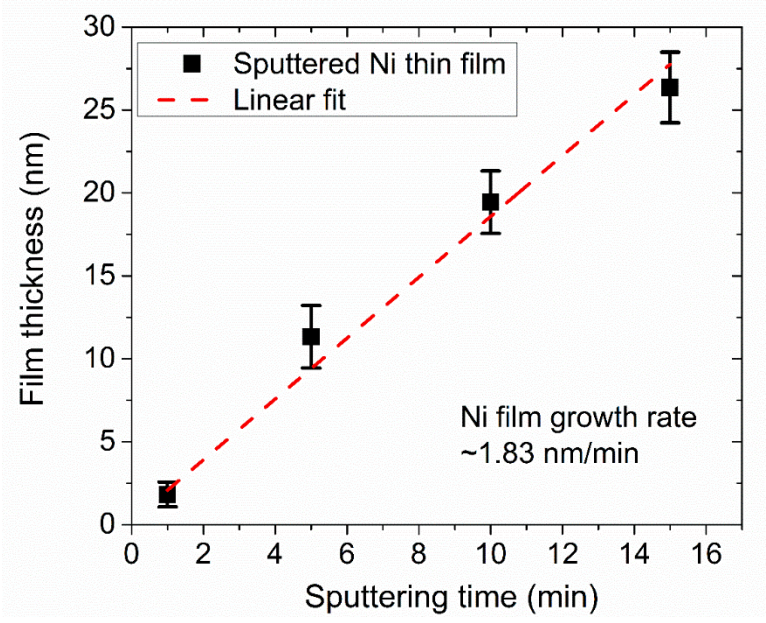

Figure S1. Relationship between Ni film thickness and magnetron sputtering time at 100 W with 7 SCCM Ar flow rate.

Setup for in-situ surface stress measurement of metal films. The charge-induced surface stress on the Ni or Au films was measured *in situ* by a multiple-beam optical stress sensor (MOSS) system (k-Space Associates Inc., USA)[3] during electrochemical processes. As illustrated in Figure 1a, the MOSS system utilized a solid state laser in conjunction with two orthogonal etalons to produce 3 × 4 arrays of parallel beams. The beams propagated through the electrolyte and were projected on to the Au mirror on the cantilever. The reflected beams were monitored by a charge coupled device (CCD) camera, and images transferred to a computer for measurements of the beam spacing with time. The beam spacing changed due to bending of the cantilever, induced by any changes of the surface stress.

For electrochemistry and stress measurement of Ni film (Figure 1a), the metal coated Si wafer with the Au mirror facing upwards was fixed at one end in a homemade electrochemical cell filled with 1M NaOH electrolyte. The Ni film was connected as the working electrode (WE) of the potentiostat (Autolab, PGSTAT302N) through a Au wire (0.25 mm in diameter). A Pt wire acted as a counter electrode (CE), and a home-made Ag/AgCl reference electrode (0.375 V vs. SHE in 1 M NaOH at room temperature, Figure S2) was inserted into the electrochemical cell just below the Ni film.

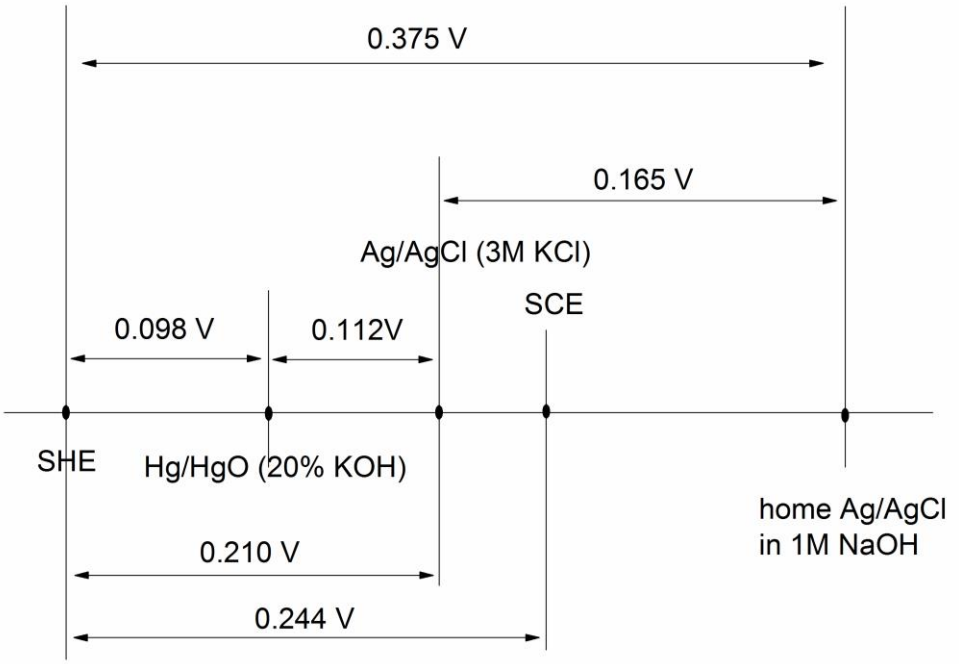

Figure S2. Illustration of home-made Ag/AgCl reference electrode against various common reference electrodes in 1M NaOH electrolyte. The home-made Ag/AgCl electrode was made by anodization of Ag wire (0.5 mm diameter, 99.99% pure) in 1M HCl solution at 0.9V for 120 seconds with another Ag wire as both counter and reference electrodes. The electrode potential was calibrated against a commercial Ag/AgCl (3M KCl) electrode (Sigma-Aldrich) in 1M NaOH solution (the same solution for electrolyte in this work). The potential of home-made electrode was stable at ~0.165 V vs. Ag/AgCl (3M KCl) even after 3 days of working.

Bending curvature determination. During cyclic voltammetry, electrochemical reactions took place on Ni film leading to a change in the Ni film surface stress change, and due to the constraint of the substrate, the cantilever then deflected. The change of bending curvature $\Delta\kappa$ of the cantilever can be expressed as:[4]

$$\Delta\kappa = \frac{\cos\alpha}{2Ln}\frac{\Delta d}{d_0} \quad \text{(S1)}$$

where d_0 is the initial beam spacing; Δd is the change of beam spacing; n is the refractive index of the electrolyte; α is the incident beam angle; L is the distance between the cantilever and the camera. $\Delta d/d_0$ ratio was measured directly from the MOSS system. From Stoney's equation,[5] the change of mean biaxial stress of a thin film coated on a much thicker substrate can be expressed as

$$\langle\Delta\sigma\rangle = \frac{Y_s h_s^2}{6(1-\nu_s)h_f}\Delta\kappa \quad \text{(S2)}$$

where Y_s and v_s are Young's modulus and Poisson's ratio of the substrate, respectively; h_s and h_f are the thickness of the substrate and the film, respectively. Here, we use surface stress Δf to represent the stress state of the film.

$$\Delta f = \langle \Delta\sigma \rangle h_f \quad \text{(S3)}$$

As presented in the main text, for Ni films, the charge-induced stress can originate at three different depth positions: (i) at the film surface by adsorbed ions in an electrochemical double-layer; (ii) in the surface region (e.g. several nm) due to redox relations involving several mono-layers of nickel hydroxide formation; and (iii) in the film "bulk" by mobile H absorption/desorption, depending on the film thickness, the hydrogen diffusion coefficient, etc, and noting that nickel hydride formation may block further H uptake.[6] Although the detailed film stress distribution may be depth dependent, because the film thickness (18 nm) is much thinner than the substrate (200 μm) the Δf determined by experiment using Equation 1 can be considered the change of average surface stress.

Setup for in-situ strain measurement of** bulk **nanoporous metal. The linear charge-induced strain of bulk nanoporous Ni was measured *in situ* in an electrochemical cell, combined with a computer-controlled dilatometer (Linseis, L75 vertical dilatometer) and a potentiostat (Autolab, PGSTAT302N). A glass push rod was connected to the displacement sensor of the dilatometer with a small constant compressive pressure (~0.2 MPa) on the top surface of the sample in order to maintain a close contact. The electrochemical cell was filled with 1M NaOH electrolyte with the nanoporous Ni as the working electrode, a piece of carbon cloth as the counter electrode, and a commercial Hg/HgO reference electrode (0.098 V vs. SHE, Sensortechnik Meinsberg, Germany). All electrode potentials presented were converted to SHE.

Method to calculate differential capacitance. C_{diff} is calculated by the following equation according to Ref. [7] .

$$C_{diff} = \frac{Y''}{2\pi f} = \frac{Z''}{2\pi f[(Z'-R_S)^2+Z''^2]} \quad \text{(S4)}$$

where Y'' is the imaginary part of the electrode admittance, Y (= $1/Z$), where $Z = Z' + jZ''$, is the impedance. R_s is ohmic resistance determined from the high frequency intercept on Z' axis in the Z' vs. $-Z''$ diagram. Z was measured by electrochemical impedance spectroscopy with a potentiostat (Autolab, PGSTAT302N).

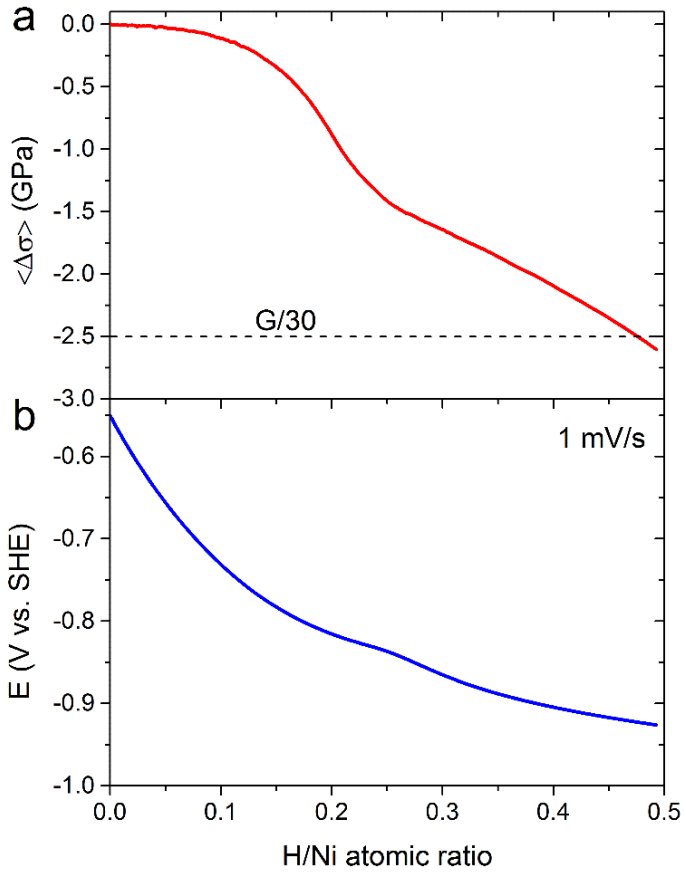

Figure S3. (a) H absorption induced change of mean biaxial stress <Δσ> in a Ni thin film as a function of H/Ni atomic ratio, where the H content was calculated from the measured charge during reduction process in cyclic voltammetry by Faraday's law. The H absorption was assumed to start at -0.55V vs. SHE (the left dash line in Figures 1f-h) until the end of the reduction processes (-0.925V vs. SHE). The horizontal dash line in (a) indicates the approximate theoretical shear strength of the Ni given by G/30 where G = 76 GPa is the shear modulus of Ni. (b) Electrode potential as a function of H/Ni atomic ratio.

Figure S3a shows the H absorption induced mean biaxial stress increased non-linearly with H uptake into the Ni film. In most of the potential region, under the lowest scan rate of

1mV s^{-1}, the induced biaxial stress was below the theoretical shear strength of the Ni. As the H/Ni ratio increased, β-nickel hydride could form, with fcc structure and a lattice constant of 3.731 Å, representing a 5.7% linear lattice expansion compared with Ni (3.530 Å).[8] The expansion of the film is restricted by the substrate and induced a compressive stress in the film. The stress was similar to that reported for H absorption into Nb films on a Si substrate.[9]

References

[1] V. Gopal, Master thesis, Technische Universität Hamburg, **2014**.

[2] N. A. Gokcen, *J. Phase Equilibria* **1991**, *12*, 313.

[3] a) M. Smetanin, Ph.D. Thesis, Universität des Saarlandes, **2010**; b) M. Smetanin, R. N. Viswanath, D. Kramer, D. Beckmann, T. Koch, L. A. Kibler, D. M. Kolb, J. Weissmüller, *Langmuir* **2008**, *24*, 8561.

[4] Q. V. Overmeere, J. F. Vanhumbeeck, J. Proost, *Rev. Sci. Instruments* **2010**, *81*, 045106.

[5] G. G. Stoney, *Proc. R. Soc. A* **1909**, *82*, 172.

[6] A. Pundt, R. Kirchheim, *Annu. Rev. Mater. Res.* **2006**, *36*, 555.

[7] V. D. Jovic, B. M. Jovic, *J. Electroanal. Chem.* **2003**, *541*, 1.

[8] N. Takano, S. Kaida, *ISIJ International* **2012**, *52*, 263.

[9] U. Laudahn, A. Pundt, M. Bicker, U. V. Hulsen, U. Geyer, T. Wagner, R. Kirchheim, *J. Alloys Comp.* **1999**, *293*, 494.